

Dear Jürg:

We thank you for taking the time to carefully critique our manuscript revision (in blue). We have edited the manuscript accordingly and have responded in red.

Dear authors

Many thanks for the revised manuscript. I am pleased with your revisions and will accept your paper pending some minor technical corrections.

Line 16: Most readers will not know where the Amu Darya river is. I suggest you add the country or some other geographical name (Hindukush?)

Ok, added "...in western High Mountain Asia,..."

Line 17: The second sentence in the Abstract is rather long and winding.

Ok, broke into two sentences

Line 21: To my knowledge, you never mention the aim of the study. It might fit in here (otherwise elsewhere in the paper).

Ok, added "To validate SWE reconstruction"

Line 22: I suggest replacing "SNOWPACK model" by "numerical snow cover model SNOWPACK"

Ok changed.

Line 24: "25 km resolution"?

Ok, added "resolution"

Line 27: "percentage of faceted layers"

Ok changed

Line 29: "peak SWE"

Ok changed

Line 30: "With regard to stratigraphy, ... was "

Deleted

Because of the changes above, here and elsewhere in the abstract a few additional deletions were made to keep the abstract word count < 250, per The Cryosphere Research article guidelines.

Lines 41-42: Please clarify. You state that climatological estimates of spatially-distributed SWE are the most important predictors of SWE. This is a bit hard to follow

Ok changed to “For example, SWE climatology is the most important predictor in machine statistical models for this region”

Line 70: “at high elevation”

Changed

Line 72: I see you point, but I don’t think ridges are appropriate locations for measuring snow.

Ok changed to “...rather than on the mountains above...”

Figure 1: Please reword: “All of the stations in Pakistan are in basins that eventually flow...”

Changed to “are in areas that eventually flow...”

Line 98: “high elevation stations”

Ok changed

Line 157: Same change suggest as in line 22.

Ok, changed. This model needs a better name.

Line 163: “accurate snow depth measurements”

Added “...snow depth...”.

Line 171: Suggest replacing “prediction” by “forecasting”. Prediction rather refers to date and location of single events.

Changed

Line 177: “Swiss Snow and Avalanche Research Institute SLF”

Changed

Line 245: I suggest introducing the abbreviation “WY” here, since you use it later on without introducing it (e.g. line 292).

Ok, added “(WY)”

Line 207: “peak snow depth”

Line 307? Changed.

Line 218: “in the top meter of the snowpack”

Line 318? Changed.

Line 322: “using the threshold sum approach”

Changed, added “sum”

Line 323: “about half of time to failure layers found in/with Compression Tests”

Changed

Line 335: I suggest you introduce somewhere here the size of the study area, i.e. that your study area is covered with 13 times 13 pixels of 25 km (325 km times 325 km [= 106'000 km²]), something along these lines.

Added “This yielded a study area of 105,625 km² (13 x 13 pixels, each 25 km² in area)”

Figure 5: I am not sure I understand, you mention: bias and error?

Deleted “error”

Also: “at AKAH stations for the median peak SWE data”

Added “on”

Figure 6: “study area ... shown in Figure 1”

Fixed “shown”

Figure 7: I suggest you refer here to the study area covered by 13 x 13 pixels of 25 km.

Changed “region” to “study area”

Line 325: placing too little SWE? Please consider rewording.

Changed “be placing” to “computing”

Line 437: “critical snowpack”

Changed “dangerous” to “critical”

Line 438: “potentially unstable snowpacks”

Added “potentially”

Line 458: To my knowledge, “lapse rate” typically relates to temperature. I guess you rather refer to the precipitation gradient with elevation.

Lapse rate can refer to change in any meteorological variable with altitude, as is discussed in the MeteIO documentation (Bavay and Egger, 2014)

Davos, 23 December 2019

Jürg Schweizer

1 **Comparison of modeled snow properties in Afghanistan, Pakistan, and Tajikistan**

2

3 Edward H. Bair¹, Karl Rittger², Jawairia A. Ahmad³, and Doug Chabot⁴

4

5 ¹Earth Research Institute, University of California, Santa Barbara, California, USA

6 6832 Ellison Hall, University of California, Santa Barbara, CA 93106-3060. correspondence

7 email: nbair@eri.ucsb.edu

8

9 ²Institute for Arctic and Alpine Research, University of Colorado, Boulder, Colorado, USA

10

11 ³Department of Civil & Environmental Engineering, University of Maryland, College Park, MD,

12 USA

13

14 ⁴independent researcher, Bozeman, MT, USA

15 ABSTRACT: Ice and snowmelt feed the Indus and Amu Darya rivers in western High Mountain
16 Asia, yet there are limited in situ measurements of these resources. Previous work in the region
17 has shown promise using snow water equivalent (SWE) reconstruction, which requires no in situ
18 measurements, but validation has been a problem. However, recently we were provided with daily
19 manual snow depth measurements from Afghanistan, Tajikistan, and Pakistan by the Aga Khan
20 Agency for Habitat (AKAH). To validate SWE reconstruction, at each station, accumulated
21 precipitation and SWE were derived from snow depth using the numerical snow cover model
22 SNOWPACK. High-resolution (500 m) reconstructed SWE estimates from the ParBal model were
23 then compared to the modeled SWE at the stations. The Alpine3D model was then used to create
24 spatial estimates at 25 km resolution to compare with estimates from other snow models.
25 Additionally, the coupled SNOWPACK and Alpine3D system has the advantage of simulating
26 snow profiles, which provide stability information. The median number of critical layers and
27 percentage of faceted layers across all of the pixels containing the AKAH stations was computed.
28 For SWE at the point scale, the reconstructed estimates showed a bias of -42 mm (-19%) at peak
29 SWE. For the coarser spatial SWE estimates, the various models showed a wide range, with
30 reconstruction being on the lower end. A heavily faceted snowpack was observed in both years,
31 but 2018, a dry year, according to most of the models, showed more critical layers that persisted
32 for a longer period.

- Deleted: until
- Deleted: when
- Deleted: For
- Deleted: model
- Deleted: Following previous work, the
- Deleted: s
- Deleted: -
- Deleted: the
- Deleted: For
- Deleted: stratigraphy, a
- Deleted:
- Deleted: is

45 1 INTRODUCTION

46 There are many parts of the world where little is known about the snowpack. This lack of
47 knowledge presents a challenge for water managers and for avalanche forecasters. Afghanistan is
48 particularly austere in this respect, as there have been no snow measurements available since the
49 early 1980s. This lack of information about the snowpack potentially creates a humanitarian crisis,
50 as snowmelt fed streams run dry in the fall without warning (USAID, 2008). Accurate historical
51 estimates of basin-wide snow water equivalent (SWE) are crucial for creating a baseline of
52 climatological conditions, which can then aid in predicting today's SWE. For example, SWE
53 climatology is the most important predictor in machine learning statistical models for this region
54 (Bair et al., 2018b).

Deleted: climatological estimates of spatially-distributed

Deleted: are

Deleted: s

55 To improve our knowledge about the snowpack in these areas, we have developed an approach
56 that requires no in situ measurements. Using satellite-based estimates of the fractional snow-
57 covered area (fSCA) and downscaled forcings in an energy balance model, we build up the
58 snowpack in reverse, from melt out to its peak, using a technique called SWE reconstruction
59 (Martinec and Rango, 1981). This technique has been shown to accurately estimate SWE in
60 mountain ranges across the world, including: the Sierra Nevada USA (Bair et al., 2016; Rittger et
61 al., 2016); the Rocky Mountains USA (Jepsen et al., 2012; Molotch, 2009); and the Andes of South
62 America (Cornwell et al., 2016)—all areas with relatively abundant independent ground validation
63 measurements. For the so called Third Pole of High Mountain Asia, and especially the
64 northwestern parts of this region, e.g. Afghanistan, Tajikistan, and Pakistan, ground-based
65 validation is challenging.

66 2 AGA KHAN AGENCY FOR HABITAT (AKAH) STATIONS

67 In 2017, we received daily manual snow depth and other meteorological measurements from
68 nearly 100 stations (Figure 1) in an operational avalanche network (Chabot and Kaba, 2016). These
69 stations are funded by the Aga Khan Agency for Habitat (AKAH) and are the first snowpack
70 measurements available, at least that we are aware of, in Afghanistan in nearly 40 years. Hence,
71 we refer to the region as the AKAH study region and the weather stations as the AKAH stations.
72 The AKAH stations contain manual daily snow depth (also called height of snow), height of new
73 (24-hr) snow, daily high and low air temperature, instantaneous wind speed/direction, rainfall, and
74 some text fields on weather and avalanche conditions. For mountainous areas, precipitation is the
75 most uncertain term in the water balance (Adam et al., 2006; Milly and Dunne, 2002) because it
76 exhibits high spatial variability and is difficult to measure with traditional gauges. Measuring snow
77 on the ground has many advantages compared to using precipitation gauges, which suffer from
78 undercatch, especially in the windy and treeless areas (Goodison et al., 1998; Kochendorfer et al.,
79 2017; Lehning et al., 2002a) typical of this part of the world. Likewise, a strength of the SWE
80 reconstruction technique is that it does not depend on precipitation measurements to build the
81 snowpack.

Deleted: Figure 1

82 Additionally, many of the AKAH stations are at high elevation, with 64 stations above 2500 m
83 and 17 stations above 3000 m. Unfortunately, most of these stations are located in deep valleys,
84 where the villages are, rather than on the mountains above and the daily resolution is too coarse to
85 use in a snow model without temporal interpolation. Additionally, many of the stations are near
86 glacierized areas which complicates spatially interpolated snow estimates, as some of the snow is
87 on top of ice. The area covered by glaciers in Figure 1 is 7.8%.

Deleted: altitudes

Deleted: exposed mountain sides or ridges

Deleted: Figure 1

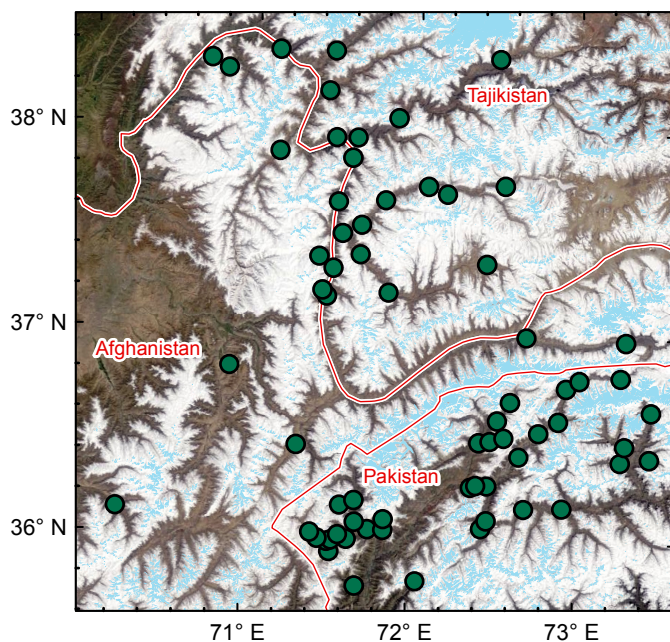


Figure 1 Study region with AKAH stations (green dots) overlaid on a MODIS true color image from 13 April 2018. Also shown are the country boundaries (red) and glacierized areas (light blue) from the Global Land Ice Measurement from Space dataset (Raup et al., 2007). All of the stations in Afghanistan and Tajikistan *are in areas that* eventually flow into the Amu Darya River. All of the stations in Pakistan *are in areas that* eventually flow into the Indus River.

95

96 Although there have been a large number of studies examining the glaciers of High Mountain Asia,
 97 there are fewer studies examining snowfall in High Mountain Asia, which is odd since
 98 hydrologically in this region, snow on land melt provides the vast majority of runoff compared to
 99 snow on ice and melting glacier ice (Armstrong et al., 2018). Many of these studies are focused on
 100 the region to the east of the AKAH study area shown in Figure 1. To our knowledge, there have
 101 been no studies on snowpack stratigraphy in the AKAH study area and we were unable to obtain
 102 any snow pit measurements from this area.

Deleted: Figure 1

103 3 LITERATURE REVIEW

104 A few studies have specifically examined snowfall in larger regions that include some of the
 105 AKAH stations, mostly for stations in the southern basins that flow into the Indus River; that is all
 106 of the stations in Pakistan. The rest of the stations in Afghanistan and Tajikistan are in basins that
 107 flow into the Amu Darya River. The most comparable study (Shakoor and Ejaz, 2019) examines
 108 the Passu catchment in the Hunza River Basin, to the east of Figure 1. As in this study (Section
 109 5.1), Shakoor and Ejaz (2019) also use the SNOWPACK and Alpine3D models. Model parameters
 110 were calibrated using a single weather station, Urdukas at 3926 m elevation near the Baltoro glacier

Deleted: Figure 1

113 (Ev-K2-CNR, 2014), with one year of precipitation measurements, using snow depth for
114 validation. The authors report overestimation of the measured snow depth at the calibration station,
115 even after questionable adjustments to the snow albedo and other model parameters. For example,
116 the snow and ice albedo is given as 0.20 to 0.30 (Table 3, Shakoor and Ejaz, 2019), which would
117 make it 0.10 to 0.20 lower than some of the lowest measured broadband albedo values for dirty
118 snow (Bair et al., 2019; Skiles and Painter, 2016). They attribute the overestimation to problems
119 with the precipitation measurements, common for high elevation stations. One problem with the
120 Urdukas station in particular is that the tipping bucket precipitation gauge is unheated, making it
121 unusable for measuring solid precipitation. Temperatures at this station were well below freezing
122 for the winter and most of the spring, which explains why no precipitation was recorded from
123 January until sometime in March during 2012, the calibration year.

124 Viste and Sorteberg (2015) study several gridded precipitation products throughout High Mountain
125 Asia, including the Indus River Basin. They report that while total precipitation was similar across
126 the products—including MERRA (Rienecker et al., 2011), APHRODITE (Yatagai et al., 2012),
127 TRMM (Huffman et al., 2007), and CRU (Harris et al., 2014)—the total snowfall varied by a factor
128 of 2 to 4. Smith and Bookhagen (2018) used 24 years (1987 to 2009) of satellite-based passive
129 microwave SWE estimates to examine trends throughout High Mountain Asia, including the Amu
130 Darya and Indus Basins. Their SWE estimates show most 25 km pixels in this region in the 50-
131 100 mm range for December through February, with a few over 100 mm in the Amu Darya (i.e.
132 all the AKAH stations in Afghanistan and Tajikistan) and none over 100 mm in the Indus (i.e. all
133 the AKAH stations in Pakistan), likely too low by an order of magnitude for some pixels given our
134 previous reconstructed SWE values and limited climate measurements in Afghanistan (Bair et al.,
135 2018b).

136 For the AKAH stations in Tajikistan, the most comprehensive snow measurements come from
137 Soviet snow surveys (mostly depth, but with some SWE and density measurements) that have been
138 digitized (Bedford and Tsarev, 2001). Most of these measurements begin in the late 1950s and end
139 around the fall of the Soviet Union, in either 1990 or 1992, making them useful for climatological
140 studies, but not for validation of modern satellite-based estimates.

141 The sole source of snow measurements in Afghanistan that were accessible to us was a table of
142 outdated WMO monthly climatological data from Kabul (el. 1791 m) and North Salang (el. 3366
143 m), showing the maximum monthly snow depth and the mean number of days with snow (Table 1
144 in Bair et al., 2018b). Again, these measurements are not useful to validate more modern snow
145 estimates.

146 There have been many other studies that have attempted to estimate basin-wide precipitation
147 (including snowfall) for larger areas that include the AKAH region, especially in the Indus. Several
148 climate studies of the Indus have focused on using lower elevation precipitation gauges, which are
149 then used to spatially interpolate basin-wide precipitation. Dahri et al. (2016) and Dahri et al.
150 (2018) have assembled perhaps the largest collection of climatological measurements covering the
151 AKAH region, mostly based on gauge measurements, as part of a study on the hydrometeorology
152 of the Indus Basin. Using undercatch corrections based on wind, often from reanalysis, they
153 increased precipitation estimates by 21% on average throughout the Indus Basin (Dahri et al.,
154 2018). For example, in the Gilgit sub-basin, they find an unadjusted precipitation estimate of 582
155 mm/year, adjusted to 787 mm/year, a 35% increase. Although some of the measurements are taken
156 from publicly available sources, as with most publications for this region, the comprehensive data
157 used are not publicly accessible.

Deleted: altitude

159 A similar but less sophisticated approach was used by Lutz et al. (2014), who used a constant
160 increase of 17% across the APHRODITE precipitation dataset which covers all of High Mountain
161 Asia. Immerzeel et al. (2015) used glacier mass balance estimates with streamflow measurements
162 as validation to show that high-altitude precipitation in the upper Indus Basin is 2 to 10 × what is
163 shown using gridded precipitation products like APHRODITE. Bookhagen and Burbank (2010)
164 estimate that snowmelt contributes 66% of annual discharge to the Indus, and averages 424 mm
165 across the basin.

166 In summary, quite a few studies have produced varying precipitation and snowfall estimates for
167 the AKAH region, with no recent in situ snow measurements from Afghanistan or Tajikistan.

168 4 PREVIOUS WORK WITH AKAH SNOW MEASUREMENTS

169 Our previous work (Bair et al., 2018b) used a simple density model (Sturm et al., 2010) based on
170 snow climatology (Sturm et al., 1995) and day of year to model SWE from the manual snow depth
171 measurements. The density model itself has -12 to 26% bias in predicting SWE. When taking into
172 account geolocational uncertainty of the reconstructed SWE estimates and uncertainty in the
173 density model, errors are on the order of 11-13% Mean Absolute Error (MAE) and -2 to 4% bias,
174 depending on the date. However, we only examined one year of the AKAH station data (2017)
175 and the high uncertainty in the density model itself begs a more sophisticated approach.

176 From recent work (Bair et al., 2018a), we have shown that the SNOWPACK (Bartelt and Lehning,
177 2002; Lehning et al., 2002a; Lehning et al., 2002b) model is capable of accurate SWE prediction
178 when supplied only with snow depth for precipitation, as well as the other requisite forcings (i.e.
179 radiation, snow albedo, temperatures, and wind speed). Over a 5-year period using hourly in situ
180 measured energy balance forcings and a snow pillow for validation at a high elevation site in the
181 western US, the [numerical snow cover model](#) SNOWPACK modeled SWE showed a bias of -17
182 mm or 1% (Bair et al., 2018a). Likewise, the success of the Airborne Snow Observatory (Painter
183 et al., 2016) has demonstrated that given accurate [snow](#) depth measurements, SWE can be well
184 modeled.

185 5 METHODS

186 Our modeling approach consisted of: a) downscaling forcings in ParBal and reconstructing SWE;
187 b) combining the downscaled forcings for each AKAH station with temporally interpolated manual
188 snow measurements; c) running SNOWPACK for each of the AKAH stations with the downscaled
189 and interpolated measurements from a) and b); and d) running Alpine3D using the output from
190 SNOWPACK, notably the hourly precipitation. In addition to predicting SWE, the
191 SNOWPACK/Alpine3D coupled model also predicts stratigraphic parameters useful for avalanche
192 [forecasting](#), thereby giving us an idea of the layering and stability in this region. For comparison,
193 we also ran the NOAH-MP land surface model over the region with widely-used forcings. We also
194 compared spatial estimates of SWE from GLDAS-2. Methods are summarized in Table 1 and
195 explained below, with more detail provided in Appendix A.

196 5.1 SNOWPACK and Alpine3D

197 SNOWPACK and Alpine3D are freely available (<https://models.slf.ch>) point and spatially
198 distributed snow models, courtesy of the Swiss [Snow and Avalanche Research Institute SLF](#).

Deleted: prediction

Deleted: Federal Snow Institute

201 SNOWPACK is the older of the two and uses finite elements to model all of the layers in a
 202 snowpack at a point.

Model	Point comparison?	Spatial comparison?	Version	Forcings	Output
ParBal	√	√	1.0	CERES 4a (radiation); GLDAS-2 (meteorological); MODSCAG/MODDRFS (snow surface properties)	Daily reconstructed SWE at 500 m; hourly downscaled forcings at 500 m, both for entire AKAH study area
SNOWPACK	√		3.5	AKAH station snow measurements; downscaled forcings from ParBal	Hourly SWE, precipitation, and other forcings for each AKAH station
Alpine3D		√	3.1	AKAH station output from SNOWPACK	Daily SWE at 25 km for entire AKAH study area
NOAH MP		√	3.6	MERRA-2	Daily SWE at 25 km for entire AKAH study area
GLDAS		√	NOAH 2.1	various	Daily SWE at 25 km for entire AKAH study area

203 *Table 1 Summary of models used. See Section 5 and Appendix A for an explanation of acronyms and further*
 204 *details.*

205 SNOWPACK has shown promising results in both operational (e.g. Lehning et al., 1999;
 206 Nishimura et al., 2005) and research applications (e.g. Bellaire et al., 2011; Hirashima et al., 2010).
 207 Previous results with SNOWPACK (Bair et al., 2018a) show high model sensitivity to
 208 precipitation, but only a 1% error in modeled SWE when using snow depth only (not total
 209 precipitation) as a forcing. Thus, given reliable snow depth measurements at each AKAH station
 210 (see Section 5.5), modeled SWE during the accumulation season is treated as having negligible
 211 uncertainty. During the ablation season (after peak SWE), uncertainty is higher. Unlike during
 212 snow accumulation events, SNOWPACK does not force its modeled snow ablation to match the
 213 measured snow depth decreases. Uncertainty in SWE during the ablation season is then largely
 214 dependent on radiative forcings (Marks and Dozier, 1992) and the broadband snow albedo (Bair
 215 et al., 2019). Here, 5% uncertainty is used, based on the MAE from SWE reconstructions using
 216 the same remotely-sensed forcings at a continental sub-alpine site (Bair et al., 2019). In the same
 217 study, a small (3%) bias in SWE was also found, but this is likely due to shortcomings with the
 218 reconstruction method and not applicable to SWE modeled with SNOWPACK. Thus, the small

Deleted: 5.4

220 bias was ignored. We acknowledge that these uncertainty estimates are themselves uncertain, e.g.
221 the reanalysis forcings could be especially poor for this region compared to those available in the
222 western US.

223 Alpine3D (Lehning et al., 2006) is essentially a spatially-distributed version of SNOWPACK with
224 a number of additional modules including: terrain-based radiation modeling, blowing snow, and
225 hydrologic modeling. Integral to Alpine3D is SNOWPACK, which is run for each pixel, as well
226 as the MeteorIO library (Bavay and Egger, 2014), which provides a large number of temporal and
227 spatial interpolation functions that can be used on forcings for Alpine3D and SNOWPACK.

228 5.2 The Parallel Energy Balance Model

229 The Parallel Energy Balance Model (ParBal) was created at UC-Santa Barbara and designed for
230 reconstruction of SWE. It is also publicly available
231 (<https://github.com/edwardbair/ParBal/releases/tag/v1.0>). Currently, ParBal is designed to use:
232 downscaled temperature, pressure, and humidity from version 2 of the Global or National Land
233 Data Assimilation System (GLDAS-2/NLDAS-2, Rodell et al., 2004; Xia et al., 2012); shortwave
234 and longwave radiation from edition 4a of the Clouds and the Earth's Radiant Energy System
235 (CERES, Rutan et al., 2015) SYN product; and time-spaced smoothed (Dozier et al., 2008; Rittger
236 et al., in press) snow surface properties from MODIS Snow Covered Area and Grain Size
237 (MODSCAG, Painter et al., 2009) and MODIS Dust and Radiative Forcing in Snow (MODDRFS,
238 Painter et al., 2012). ParBal is run hourly at 500 m spatial resolution and forcings are adjusted for
239 terrain and elevation. The main output is the residual energy balance term, which is assumed to go
240 into melt when positive during the ablation phase after cold content is overcome (Jepsen et al.,
241 2012). This residual melt term is then summed in reverse during periods of contiguous snow cover
242 and multiplied by the fSCA to spread the snow spatially. The errors in SWE from ParBal are
243 mostly from fSCA and the radiative forcings. Errors and details on ParBal are covered extensively
244 in Bair et al. (2016) and Rittger et al. (2016). In the supplement for Bair et al. (2018b), the errors
245 arising from using GLDAS-2 and CERES 4a (available worldwide but at coarser spatial resolution)
246 vs. NLDAS-2 are specifically evaluated. Using three years of basin-wide SWE estimated by the
247 Airborne Snow Observatory in the upper Tuolumne Basin, California USA, the MAE for ParBal
248 was 25 mm or 26% (Bair et al., 2018b).

249 5.3 Global Data Assimilation System 2 (GLDAS-2)

250 For comparison, we also include the SWE estimates from GLDAS-2 (Noah). SWE from GLDAS-
251 2 has been shown to be comparable to estimates from other reanalysis datasets, but negatively
252 biased by about 60% in comparison to higher spatial datasets with assimilation from snow station
253 measurements (Broxton et al., 2016).

254 5.4 NOAH Multi-Parameterization (MP)

255 The NOAH-MP v3.6 (Ek et al., 2003; Niu et al., 2011) land surface model, forced using MERRA-
256 2 (Gelaro et al., 2017), was used to simulate the hydrologic cycle over the study area and provide
257 SWE estimates for comparison with ParBal and the Alpine3D output. NOAH-MP was selected
258 due to its detailed representation of the snowpack relative to other land surface models. The model
259 subdivides the snowpack into up to three layers with associated liquid water storage and
260 melt/refreeze capability (Niu and Yang, 2004; Yang and Niu, 2003). It incorporates the exchange

261 of heat and moisture through the snowpack between the land surface and the atmosphere. In a
262 model intercomparison study using a 2 km spatial resolution regional climate model for forcings,
263 Chen et al. (2014) show that NOAA-MP modeled peak SWE at SNOTEL sites in Colorado, USA
264 with a -7% bias.

265 5.5 Use of AKAH station measurements

266 We modeled daily SWE at the AKAH stations during the 2017 and 2018 water years (WY)
267 primarily using the manually measured height of snow (HS), also called snow depth, combined
268 with our downscaled energy balance parameters (for downscaling methodology see Bair et al.,
269 2018b; Bair et al., 2016; Rittger et al., 2016). To our knowledge, no quality control was performed
270 on the AKAH station measurements before we received them. We choose the manual HS and new
271 (24-hr) snow (HN) as the only variables to use from the AKAH stations. The HS appeared to be
272 the most reliably measured, as that only requires reading a value from a master snow depth stake.
273 Apart from spurious drops or missing values (see below), the HS measurement appeared consistent
274 and believable at most of the stations, implying an accurate snow depth record. The HN was used
275 to correct a data entry problem in 2017 that we discuss below. The reliability of the other
276 measurements (instantaneous wind speed/direction, maximum/minimum temperature, and
277 rainfall) was questionable. For example, we were not provided with sensor or measurement
278 metadata, e.g. sensor make/model, measurement height, and whether or not the temperature sensor
279 was shielded from shortwave radiation. These other measurements taken daily were also of limited
280 value for interpolation to hourly values (see item 3 below). Thus, these other measurements were
281 not used.

282 The AKAH dataset had a number of shortcomings that we list here along with how we addressed
283 them.

- 284 1) Some of the stations recorded no snow at all, especially in the dry 2018 year, or had obvious
285 problems, such as weeks of missing measurements, so they were excluded. For 2017, 52 (54%)
286 of stations were used. For 2018, 41 (46%) stations were used.
- 287 2) There were spurious drops in the HS measurements. The drops were clearly cases of missing
288 values being filled with zeros. These measurements were manually flagged and converted to
289 null values for interpolation, see below.
- 290 3) The daily measurements had to be interpolated to hourly values. For the most part we used
291 linear interpolation, although this is not ideal during snow accumulation since it's almost never
292 the case that snowfall is uniform over a 24-hr period. This is a problem that affects the accuracy
293 of snow settlement estimated by SNOWPACK. There were two cases where other interpolation
294 methods were used. If there were several days of missing values, we used a nearest neighbor
295 interpolation to fill in the missing daily values, followed by a linear interpolation from daily to
296 hourly measurements such that we assumed all the new snow fell in a 24-hr period. The other
297 case was for days where the linear interpolation would yield a value below the minimum
298 threshold hard coded into SNOWPACK (0.5cm/hr) for the first accumulating snowfall on bare
299 ground. In this case, a previous neighbor interpolation was used in such a way that the entire
300 snowfall occurred in the last hr prior to the next day's measurement.
- 301 4) We found the AKAH stations suitable for snow on the ground measurements, but not for
302 rainfall or total (solid+liquid) precipitation. This was only an issue for the Alpine3D snow
303 modeling, as snow measurements were being extrapolated to higher elevations than the AKAH

304 stations (Section 6.2), thus at these higher elevations, snow accumulated earlier and melted
305 later than at the lower AKAH stations.

306 Given the near total lack of canopy cover in the region, we suspected substantial undercatch from
307 rain gauges. Using the wind speed, an undercatch correction would have been possible given more
308 information on the gauges (e.g. orifice opening diameter and whether or not a shield was present),
309 however this instrument metadata was not available to us. Likewise, we did not know if the gauges
310 were heated or not.

311 Further, the time period for recording measurements from the stations was not consistent. In WY
312 2017, measurements began being reported on 10 November 2016 and were reported until 24
313 November 2017. However, in WY 2018, measurements weren't reported until 1 December 2017
314 and no station measurements were reported past 1 April 2017. The reporting period likely covered
315 all the snowfall events, but not all the precipitation events.

316 To address the rainfall measurement and reporting issues, we used GLDAS NOAH v2.1 (Rodell
317 et al., 2004) rainfall + snowfall from the nearest grid cell (1/4° spatial / 3 hr temporal resolution)
318 to fill in precipitation prior to the first measurements in each water year, and after 4-1 for both
319 water years. We did not account for rain from 10 November 2016 to 1 April 2017 and from 1
320 December 2017 to 1 April 2018; instead we relied on the modeled precipitation from SNOWPACK
321 using snow depth. The AKAH station observations show that rain during this time period was rare.

322 5) A database problem prevented snow heights > 100 cm from being entered into the database for
323 a few days in 2017. This problem became apparent during February 2017, when the Nuristan
324 avalanches took place (United Nations, 2017), as that is the first time that most stations
325 recorded values > 100 cm. Values were shown as 100 cm on multiple days followed by values
326 > 100 cm. To address this issue, we flagged all the values equal to 100 cm prior to peak [snow](#)
327 depth in 2017, then marked those as null values. We then filled those null values using the
328 cumulative sum of new snow during that time.

329 5.6 Analysis of modeled snow profiles

330 For holistic measures of the snow profiles modeled in Alpine3D, we used two metrics from
331 Bellaire et al. (2018): 1) fraction of facets and 2) number of critical layers. Fraction of facets is the
332 height of all the layers containing faceted crystals, i.e. International Classification for Seasonal
333 Snow on the Ground primary codes FC, DH, and SH (Fierz et al., 2009), divided by the height of
334 the snowpack. The number of critical layers was computed using a threshold sum approach
335 (Schweizer and Jamieson, 2007) with modifications for simulated profiles (Monti et al., 2014
336 Table 1). In each profile, 6 different variables (grain size, difference in grain size, hardness,
337 difference in hardness, grain type, and depth) in the top meter of [the snowpack](#) (from the surface)
338 were checked against threshold values. Layers exceeding 5 or more thresholds were classified as
339 critical.

340 The fraction of facets metric does not have a validation study, but faceted layers are a weak crystal
341 form and are responsible for 43% (Bair et al., 2012) to 67% (Schweizer and Jamieson, 2001) of
342 investigated avalanches. Layers classified as critical using the threshold [sum](#) approach above
343 corresponded to failure layers about [half of the time to failure layers found with Compression Tests](#)
344 (Monti et al., 2014), [an in situ snowpack stability test](#) (Jamieson, 1999; van Herwijnen and
345 Jamieson, 2007).

Deleted: height

Deleted: ½

Deleted: in Compression Tests

Deleted: , an in situ snowpack stability test

350 5.7 Spatial scale for comparisons

351 Because ParBal is the only model run at 500 m spatial resolution and all the other models were run
 352 at ~ 25 km, it is the only model appropriate for point comparisons, although point to area problems
 353 are still an issue. To address the geolocational uncertainty for the gridded MODIS products, which
 354 can be up to one ~500 m pixel (Tan et al., 2006; Xiaoxiong et al., 2005) and spatial variability of
 355 the snow, we used a 9-pixel neighborhood centered on each AKAH station and chose the best fit
 356 to the SNOWPACK modeled SWE. This approach has been used in previous work (Bair et al.,
 357 2018b; Rittger et al., 2016). We also include the high and low SWE values in that surrounding 9-
 358 pixel neighborhood to bound the uncertainty.

359 For all of the other model comparisons, we resampled all of the model output to a UTM (Zone
 360 43S) grid with 25 km pixels, close to the native resolution of the NOAA-MP and GLDAS2 grid
 361 used (0.25°). This yielded a study area of 105,625 km² (13 x 13 pixels, each 25 km² in area). The
 362 ParBal output had to be significantly upscaled from 500 m to 25 km using Gaussian Pyramid
 363 reduction (Burt and Adelson, 1983) in steps with bilinear interpolation for the final step.

364 6 RESULTS AND DISCUSSION

365 The relationships between the components are summarized in Figure 2. The results discussed
 366 below are comparisons of: 1) SWE and 2) snow stratigraphy across a) all of the AKAH stations
 367 (points) and b) the entire study region.

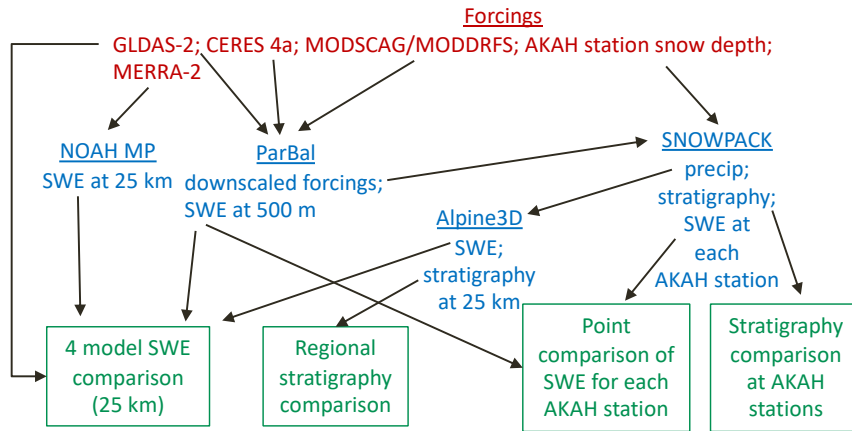


Figure 2 Summary of relationships between the various components. Forcings are shown in red, models and selected outputs are shown in blue, and the comparisons discussed below are shown in green. The black arrows show the direction of inputs.

368

369 6.1 Point comparisons between SNOWPACK and reconstructed SWE

370 A first step for any SWE reconstruction comparison is to determine when the ablation season starts.

371 This varies for different years and at different sites (e.g. Margulis et al., 2016). Using the

373 SNOWPACK modeled SWE, we can examine the peak SWE dates for both years for all of the
 374 AKAH stations (Figure 3ab). Peak SWE dates vary across the stations and years, but the median
 375 values between years are a week apart, 19 February 2017 and 26 February 2018. Thus, we use
 376 those dates for our comparisons.

Deleted: Figure 3

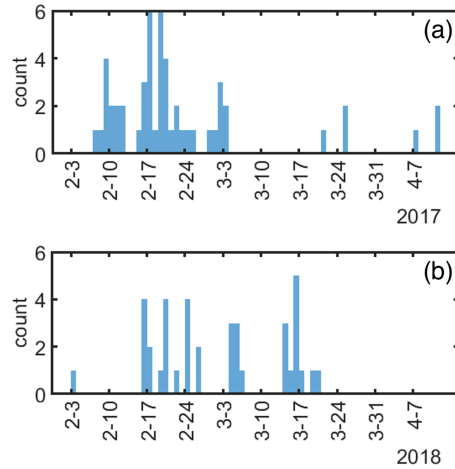


Figure 3 Peak SWE dates, modeled by SNOWPACK for 2017 (a) and 2018 (b) for each of the AKAH stations. The median peak SWE dates are 19 February 2017 and 26 February 2018. N=52 and 41 AKAH stations used for 2017 and 2018.

377

378 To create a holistic comparison for all the stations across the ablation period, mean SWE values
 379 were computed and plotted for each day during the ablation season (Figure 4). For the
 380 reconstructed SWE on 19 February 2017, the bias is -77 mm (-28%). For the reconstructed SWE
 381 on 26 February 2018, the bias is -6 mm (-9%). Thus, together these biases average to -42 mm (-
 382 19%). The high/low values in the 9-pixel neighborhood show the wide spatial variation in SWE
 383 estimates, and are to be expected in these deep valley sites (Section 6.2). The increases in
 384 reconstructed SWE during the ablation season are caused due to differences in how melt is summed
 385 for any given pixel. In ParBal, melt is only summed during periods of contiguous snow cover. This
 386 means that if a pixel containing an AKAH station has no snow on it at some point during the
 387 ablation season, but then snow is detected, it causes an increase in the mean SWE. This is called
 388 an ephemeral snow event, i.e. snow that disappears and reappears. For a more in depth examination
 389 of the error at individual stations, a box plot is shown for the median peak SWE dates for both
 390 years (Figure 5). The median bias of the reconstructed SWE is -11 mm (-14%).

Deleted: Figure 4

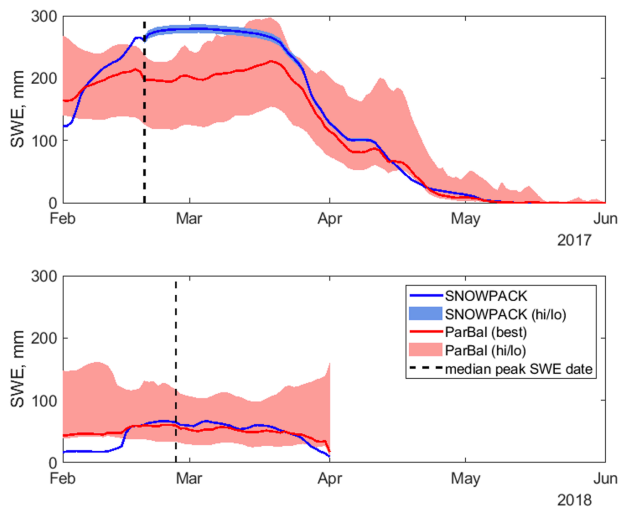


Figure 4 Mean SWE for 2017 (a) and 2018 (b) modeled at all of the AKAH stations using SNOWPACK (blue lines) compared to reconstructed SWE from ParBal using a best of 9-pixel approach (red lines). Also plotted is the median peak SWE date. The hi/lo bounds (filled areas) represent uncertainty. For ParBal, uncertainty is expressed as the range of values in the 9 pixel neighborhood. For SNOWPACK, uncertainty is 5% of the modeled SWE during the ablation season. See Sections 5.1 and 5.2 for details. The modeled SWE values end abruptly on 1 April 2018 because the AKAH stations stopped reporting due to drought conditions. The number of stations used is the same as in [Figure 3](#).

Deleted: Figure 3

393
394

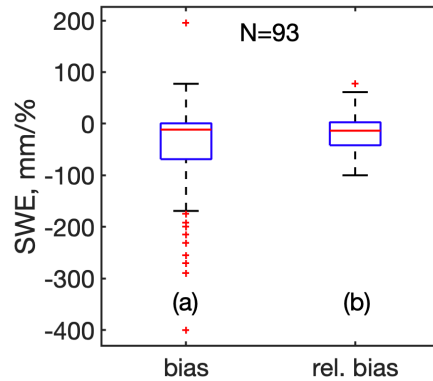


Figure 5 Bias (a) and relative bias (b) for ParBal reconstructed SWE vs Alpine 3D modeled SWE at AKAH stations on the median peak SWE date for both years, where bias here is ParBal SWE – Alpine 3D SWE.

Deleted: error

395

396 6.2 Four model spatial comparisons

397 The AKAH stations are lower than the average elevation for the region. The average elevation of
 398 the AKAH stations is 2619 m (1735 to 3410 m). But when the 500 m DEM is upscaled to 25 km,
 399 the average elevation of the pixels containing the AKAH station is 3858 m with a range of 2517
 400 to 4764 m. This has two important implications: 1) much of the higher elevation snowfall is being
 401 extrapolated and 2) the higher elevation causes the peak SWE date to move forward in time. The
 402 median peak SWE dates for the (N=169) 25 km pixels encompassing the study area are 5 May
 403 2017 and 3 May 2017. Thus, we use the median of the two to compare our reconstructed SWE
 404 values (Figure 6ab, Figure 7a-d, and supplementary video).

405 Striking is the range between models. NOAH-MP has the highest peaks (562 mm in 2017 and 331
 406 mm in 2018), but is among the first to melt out. The reconstructed SWE from ParBal only shows
 407 minor variation between the 2017 peak (240 mm) and the 2018 peak (206 mm). ParBal and
 408 GLDAS-2 melt snow out latest in both years. This is especially true for ParBal in 2017, where the
 409 supplementary video shows that ParBal has snow cover over more pixels that persists for longer
 410 into the melt season, but is lower in SWE than the other models. The Alpine 3D model shows the
 411 second highest peak SWE in 2017 (469 mm), but the lowest peak (165 mm) in 2018. The
 412 comparatively higher values from NOAH-MP could result from relatively high precipitation
 413 estimates from its MERRA2 precipitation forcings. Similarly, Viste and Sorteberg (2015) report
 414 that MERRA (version 1) showed higher snowfall in the Indus Basin than any other reanalysis or
 415 observation-based forcings dataset.

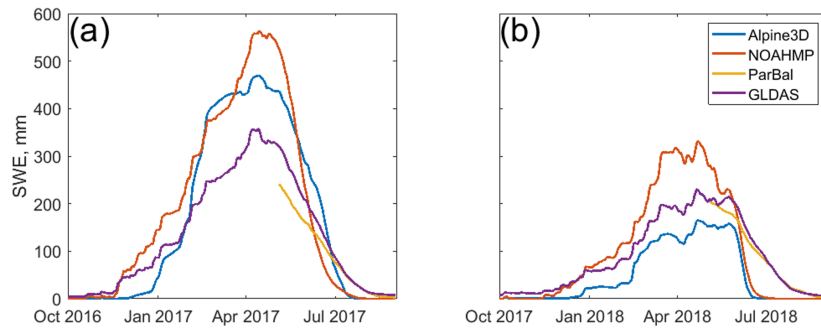


Figure 6 Time series of mean SWE for four snow models across the study area (13x13x25 km pixels) shown in Figure 1, for 2017 (a) and 2018 (b). The reconstructed SWE from ParBal (yellow) goes back to 4 May, the median peak SWE date for both years, since reconstruction is only valid during the ablation season.

Deleted: Figure 1

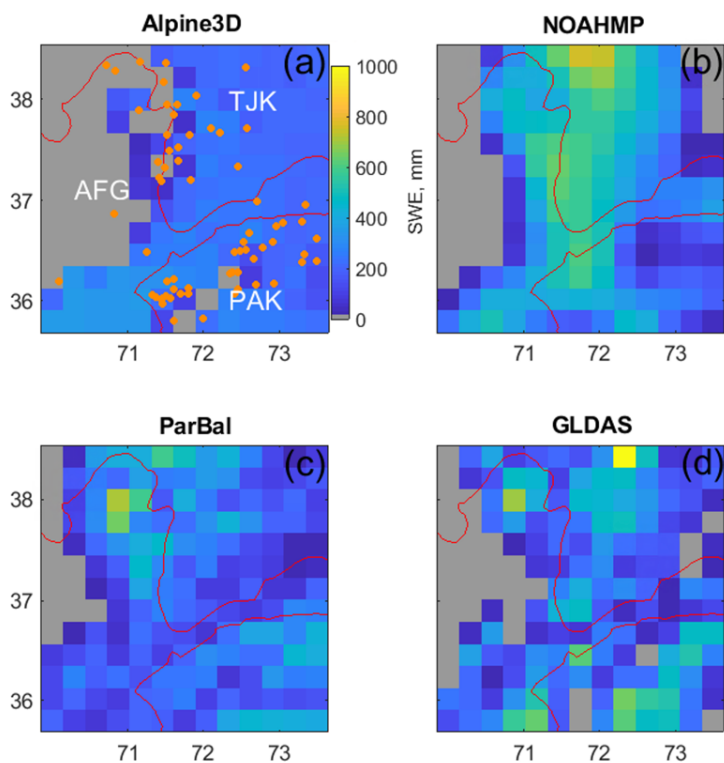


Figure 7 Four model (a-d) spatial comparison for the study area on 4 May 2018. The white letters are: AFG–Afghanistan; TJK–Tajikistan; and PAK–Pakistan. Also shown in (a) are the locations of the AKAH stations (orange points). This is a frame from a video sequence available as supplementary material.

Deleted: region

417 Since Alpine3D is relying heavily on extrapolation of SWE, we suggest its mean SWE values
 418 plotted in Figure 6 could have higher uncertainty than some of the other models. For example, the
 419 Alpine3D pixels seem to melt out early compared to the other models, especially ParBal, which is
 420 the only model relying on satellite-based estimates of fSCA (see supplementary video). Thus,
 421 Alpine3D may computing too little SWE in cold, high elevation areas that melt slowly. These
 422 problems are all indicative of stations that are located in valley bottoms and that only cover the
 423 lowest elevations across these 25 km pixels.

Deleted: be placing

425

427 The ParBal results are confounding given that the agreement between the modeled SWE from
428 ParBal and SNOWPACK at individual AKAH stations (Figure 4ab) is much better for both 2017
429 and 2018.

Deleted: Figure 4

430 For insight into potential biases in the modeled spatial SWE from ParBal, we carefully studied the
431 snow-covered area (SCA, not just for 2017 & 2018, but since 2001), the potential melt (i.e. the
432 melt if a pixel were 100% snow covered), and the melt from glacierized areas (light blue in Figure
433 1). We did not find any errors in the model, its parameters, or its forcings. Thus, it is possible that
434 the ParBal SWE is low-biased in 2017 for reasons that we could not discern, or that the other
435 models are high biased. Of note is that the 2017 & 2018 SCA (Figure 8 purple and orange) is very
436 similar for both years during the ablation period, especially at the end of the ablation season.

Deleted: Figure 1

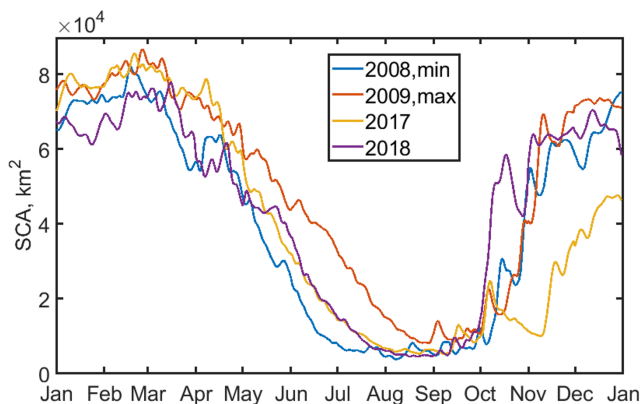


Figure 8 Time series of snow covered area from spatially and temporally interpolated MODSCAG (Rittger et al., in press), an input for ParBal, for four selected years across the region. Years 2008 and 2009 had the lowest and highest values on July 1 over the period of record from 2001 to 2018, while 2017 and 2018 comprise the AKAH station study period.

437 Since pixels do not contribute uniformly to melt, SCA alone cannot be used to predict SWE, but
438 in general years with less snow have lower SCA values towards the end of the ablation season.
439 Figure 8 shows that 2017 and 2018 were similar in terms of SCA from April through melt out.
440 Thus, the large difference between 2017 and 2018 for the AKAH station SWE, but small
441 differences in SCA and spatially-averaged reconstructed SWE, suggest that 2017 may have been
442 a larger snow year at the lower elevations where the AKAH stations are, but similar to 2018 at the
443 higher elevations.
444

445 6.3 Stratigraphy and stability

446 The simulated snow profiles from the AKAH stations (Figure 9ab) and the 25 km pixels containing
447 the AKAH stations (Figure 10ab) show very different snowpacks. Because of the induced increase
448 in elevation from scaling (e.g. from an average of 2619 m to 3858 m, Section 6.2), the 25 km pixels
449 show a deeper, but more faceted snowpack with critical layers that persist for a month or longer.
450 In 2017, for the median AKAH station values, the snowpack reaches a maximum of 76% facets

453 on January 21 (Figure 9a). In 2018, the snowpack reaches a maximum of 71% facets (Figure 9b).
 454 There were no critical layers simulated. In contrast, for the median values in the 25 km pixels for
 455 both years, the height of snow (HS) is approximately $2 \times$ that for the stations (Figure 10ab). The
 456 snowpack reaches a maximum of 94% facets in 2017, with one critical layer persisting for 35 days
 457 (Figure 10a). The snowpack in 2018 reaches 95% facets with 1 or 2 critical layers persisting for
 458 80 days (Figure 10b). During the Nuristan avalanches on 4 February to 7 February 2017 that killed
 459 over 100 people (United Nations, 2017), the AKAH stations show the largest 3-day snowfall of
 460 the study period (Figure 9a) and the results for the 25 km pixels show that large snowfall occurring
 461 on top of the only critical layer of the season (Figure 9b). That is a classic avalanche scenario, i.e.
 462 a large snowfall on a weak snowpack.

463 In lieu of any type of snow profile from this region, these profiles paint the best picture of the snow
 464 conditions available. A relatively stable snowpack seems to be present in the valleys, where the
 465 AKAH stations are located. But at the higher elevations, the simulated profiles show a more **critical**
 466 snowpack. This is especially serious considering these villages are in the runout zones of these
 467 **potentially** unstable snowpacks. In some cases, several thousand meters of vertical relief loom
 468 above the villages. For example, Yarkhun Lasht (36.795N 73.022E, el. 3249 m) in Pakistan is
 469 flanked by 6500 m peaks on both side of its valley.

Deleted: dangerous

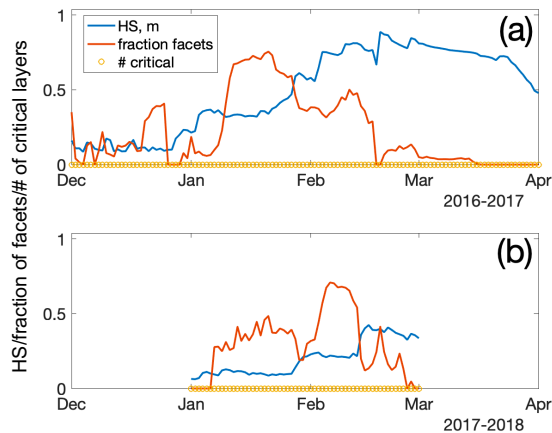


Figure 9 Stratigraphy summary of the AKAH stations for 2017 (a) and 2018 (b). Plotted are the median: height of snow (HS); fraction of the snowpack containing facets; and number of critical layers. The number of stations used to compute the medians varied due to snow coverage.

470

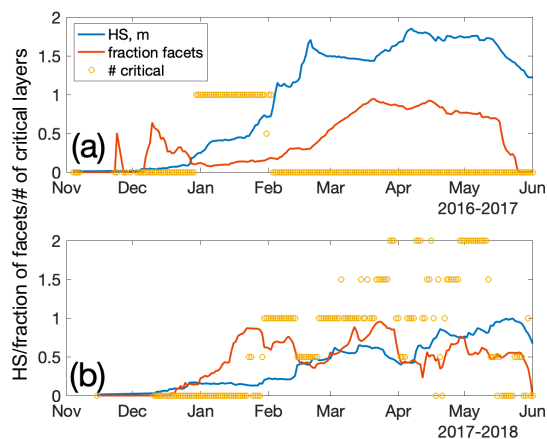


Figure 10 Stratigraphy summary of the (13x13) 25 km pixels containing AKAH stations for 2017 (a) and 2018 (b). Plotted are the median: height of snow (HS); fraction of the snowpack containing facets; and number of critical layers.

473

474 7 CONCLUSION

475 Knowledge of the snowpack in northwestern High Mountain Asia is poor. This area is subject to
 476 droughts and threatened by snow avalanches. Both problems can be aided by improved knowledge
 477 of the snowpack. Thanks to a novel operational avalanche observation network, there are now
 478 daily snow measurements at a number of operational weather stations in this austere region. In this
 479 study, two years of daily snow depth measurements from these stations were combined with
 480 downscaled reanalysis and remotely-sensed measurements to force a point and spatially distributed
 481 snow model. Compared to a previous effort (Bair et al., 2018b), this study represents a substantial
 482 improvement in SWE modeling for the region, and a first attempt to characterize region-wide snow
 483 stratigraphy. At the point scale, SWE estimates from a reconstruction technique that does not use
 484 precipitation or in situ measurements compared favorably. At the regional scale, four models
 485 showed a wide spread in both peak SWE and melt timing. For the models that rely on in situ
 486 precipitation measurements, a major challenge is spatial extrapolation, as many of the stations are
 487 located in deep valleys. Adding measurements from the mountains above would facilitate more
 488 realistic lapse rates, but these measurements do not currently exist, although they would be
 489 beneficial both for operational avalanche safety and for scientific studies.

490 In the regional comparison, SWE estimates from ParBal were on the low end, but given the model
 491 spread it is difficult to form a consensus estimate. We plan additional in situ validation at other
 492 sites in High Mountain Asia to continue to assess the performance of ParBal there.

493 The simulated profiles showed very different snowpacks. At the point scale at lower elevations in
 494 the valleys, profiles showed fewer facets and almost no critical layers, while at the regional scale

495 for higher elevations, the profiles showed heavily faceted snowpacks with critical layers that
496 persisted throughout the winter and spring.

497 8 CODE AND DATA AVAILABILITY

498 The code for ParBal is accessible at: <https://github.com/edwardbair/ParBal>

499 The code for MeteoIO, SNOWPACK, and Alpine3D are accessible at: <https://models.slf.ch/>

500 The code for NOAH-MP is accessible at: [https://ral.ucar.edu/solutions/products/noah-](https://ral.ucar.edu/solutions/products/noah-multiparameterization-land-surface-model-noah-mp-lsm)
501 [multiparameterization-land-surface-model-noah-mp-lsm](https://ral.ucar.edu/solutions/products/noah-multiparameterization-land-surface-model-noah-mp-lsm)

502 The GLDAS-2 and MERRA-2 forcings are accessible at: <https://disc.gsfc.nasa.gov/>

503 The reconstructed SWE and melt cubes are accessible at:
504 <ftp://ftp.snow.ucsb.edu/pub/org/snow/products/reconstruction/h23v05/500m/>

505 Unfortunately, the AKAH measurements are not publicly available due to security concerns.
506 Requests for the dataset should be made through The Aga Khan Agency for Habitat
507 (<https://www.akdn.org>).

508 **APPENDIX A Detailed model forcings and parameters**

509 *PARBAL*

510 ParBal was configured and forced as described in Bair et al. (2018b); Bair et al. (2016). The model
 511 time step was 1 hr. The DEM used was the ASTER GDEM version 2 at 1 arc sec (NASA JPL,
 512 2011), while the canopy type and fraction were taken from the Global Land Survey at 30 m (USGS,
 513 2009). The shortwave and longwave forcings were downscaled from the CERES SYN edition 4a
 514 1°/1 hr product (Rutan et al., 2015), while the air temperature, specific humidity, air pressure, and
 515 wind speeds were downscaled from the GLDAS NOAH version 2.1 0.25°/3 hr product (Cosgrove
 516 et al., 2003). Time-space smoothed (Dozier et al., 2008; Rittger et al., in press) fSCA and grain
 517 size from MODSCAG (Painter et al., 2009) was combined with the visible albedo degradation
 518 from dust in MODDRFS (Painter et al., 2012) to produce snow hourly snow albedo.

519 *NOAH-MP*

520 NOAH-MP v3.6 was run in retrospective mode within the NASA Land Information System (LIS)
 521 framework. A state vector ensemble (total 30 replicates) was generated by perturbing the forcings
 522 to account for the state uncertainty during forward propagation of the model. MERRA-2 (Gelaro
 523 et al., 2017) forcings were utilized with bilinear spatial and linear temporal interpolation. The
 524 model was run on an equidistant cylindrical grid with 0.25° spatial resolution and a 15 min model
 525 timestep. The spin-up time extended from May 2002 to May 2016 while the study period was from
 526 June 2016 to October 2018. The number of maximum layers in the snowpack was 3. Table A1
 527 provides details of the NOAH-MP scheme options selected. Further details regarding each scheme
 528 and relevant references can be found at: [https://ral.ucar.edu/solutions/products/noah-](https://ral.ucar.edu/solutions/products/noah-multiparameterization-land-surface-model-noah-mp-lsm)
 529 [multiparameterization-land-surface-model-noah-mp-lsm](https://ral.ucar.edu/solutions/products/noah-multiparameterization-land-surface-model-noah-mp-lsm).

Physical process/ parameter	Scheme used
Elevation data	SRTM Native
Landcover data	MODIS Native (IGBP/NCEP)
Slope, Albedo and Greenness data	NCEP Native
Bottom temperature (lapse-rate correction)	ISLSCP1
Vegetation	dynamic
Canopy stomatal resistance	Ball-Berry
Runoff and groundwater	SIMGM
Surface layer drag coefficient	M-O (General Monin-Obukhov similarity theory)
Supercooled liquid water and frozen soil permeability	NY06
Radiation transfer	gap=F(3D;cosz)
Snow surface albedo	BATS (Biosphere-Atmosphere Transfer Scheme)

Rainfall and snowfall	Jordan91
Snow and soil temperature time	semi-implicit
Lower boundary of soil temperature	Noah

530 *Table A1 Noah-MP v3.6 physical parametrization scheme options utilized in this study.*

531 *SNOWPACK*

532 SNOWPACK v3.50 was run in research mode at a 15 min timestep with hourly outputs for each
533 of the AKAH stations. Hourly forcings were computed by combining temporally interpolated snow
534 depth from the AKAH manual measurements with: air temperature, incoming shortwave, reflected
535 shortwave, incoming longwave, wind speed, and relative humidity from the downscaled ParBal
536 outputs, as described in Section 5.2. SNOWPACK was only run for periods when measurements
537 from the AKAH stations were available, Nov/Dec to April/May, depending on the year.

538 Plots were assumed to be level, so forcings without terrain correction were applied except for
539 shading when the sun was below the local horizon, e.g. a mountain blocking the sun (Dozier and
540 Frew, 1990). The wind direction, which is not available in GLDAS-2, was fixed at the mean value
541 from the daily AKAH instantaneous values. The ground temperature was set as the minimum of
542 the air temperature or -1.5°C when snow cover was present.

543 Aside from setting required parameters and values for inputs and outputs, changes to default
544 parameters that affected model output are provided in Table A2:

Parameters	Value	Description
TS_DAYS_BETWEEN	0.014666 days	Output hourly values
PRECIP_RATES	FALSE	Output is provided a summed precipitation over the output timestep (1 hr)
SW_MODE	BOTH	Both incoming and reflected (incoming x albedo) are provided
HEIGHT_OF_METEO_VALUES	2 m	Height of meteorological measurements
HEIGHT_OF_WIND_VALUE	2 m	Height of wind measurements
ENFORCE_MEASURED_SNOW_HEIGHTS	TRUE	Precipitation is calculated using HS
ATMOSPHERIC_STABILITY	NEUTRAL	Neutral conditions are often present in moderate to high wind speeds for mountain terrain (Lehning et al., 2002a; Mitterer and Schweizer, 2013)
MEAS_INCOMING_LONGWAVE	TRUE	Default is to estimate emissivity of the air and incoming longwave from

		other measured parameters (FALSE). Here we provide longwave forcings (TRUE).
--	--	--

545 *Table A2 Model parameters for SNOWPACK*

546 *ALPINE3D*

547 Alpine3D version 3.10 was run using with the outputs produced by SNOWPACK as forcings for
548 each of the AKAH stations at 25 km resolution. The DEM and land cover (incorrectly labeled land
549 use in the Alpine3D documentation) data were upscaled from the ParBal data. Alpine3D was run
550 at an hourly timestep using hourly forcings, with daily outputs using the “enable-eb” switch. Other
551 switches were set to off, the defaults. The “enable-eb” switch computes the terrain radiation with
552 shading and terrain reflections (see Alpine 3D documentation at <https://models.slf.ch> for a
553 description).

554 To extend the length of the model runs, for each AKAH stations, GLDAS-2 precipitation was
555 appended to periods prior to the first AKAH observation for the year and after the last, as described
556 in Section 5.5.

557 The forcings were hourly: incoming shortwave, incoming longwave, air temperature, relative
558 humidity, wind speed, wind direction, reflected shortwave, accumulated precipitation, and ground
559 temperature.

560 Critical to Alpine3D are the interpolation methods from MeteoIO to spatially distribute
561 precipitation and other forcings. We found the modeled SWE to be highly dependent on the spatial
562 interpolation of precipitation. Our initial approach was to explore local (i.e. with a given radius
563 from a station) and regional (i.e. all AKAH stations) lapse rates in the measured snow depth and
564 modeled precipitation from SNOWPACK. We found almost no correlation in many of the
565 measurements, not surprising given the complexity of the terrain and likely existence of
566 microclimates with substantial influence on precipitation. Without having a good validation source
567 for spatial precipitation (as is the case for all of High Mountain Asia), we selected an interpolation
568 method that yielded relatively smooth results, but showed increases in precipitation with elevation.

569 Ultimately, we decided to use an inverse distance weighting scheme with elevation detrending
570 (IDW LAPSE) and a multilinear option. For this method, the input data are detrended, then the
571 residuals are spatially interpolated according to an inverse distance weighting scheme. The
572 detrending uses a multiple linear regression with northing, easting, and altitude. The linear
573 regression has an iterative method for removing outliers. Finally, values at each cell are retrended
574 using the multiple linear regression and added to the interpolated residuals.

575 A summary of the interpolation methods, all of which are defined in the MeteoIO documentation
576 (Bavay and Egger, 2014), is given in Table A3.

Forcing	Spatial interpolation method	Description and notes
Air temperature	IDW_LAPSE	Inverse distance weighting with elevation detrending.

Deleted: 5.4

Accumulated precipitation	IDW_LAPSE with multilinear option set to TRUE	See notes above
Relative Humidity	LISTON_RH	See Liston and Elder (2006)
Precipitation phase	PPHASE	Simple splitting at 274.35K
Wind speed	IDW_LAPSE	See above
Incoming longwave radiation	AVG_LAPSE	Average filling with elevation lapse rate
Wind direction	CST	Constant, fixed at average value from AKAH station instantaneous measurements
Pressure	STD_PRESS	Standard atmospheric pressure with elevation

578 *Table A3 Spatial interpolation methods for Alpine3D*

579 The same parameters as in Table A2 for SNOWPACK were used in Alpine3D with changes shown
580 in Table A4. Other parameters were defaults.

Parameters	Value	Description
CALCULATION_STEP_LENGTH	60 min	1 hr model timestep
ENFORCE_MEASURED_SNOW_HEIGHTS	FALSE	Use accumulated precipitation estimate from SNOWPACK

581 *Table A4 Model parameter changes for Alpine3D from Table A2*

582 AUTHOR CONTRIBUTION

583 DC provided the AKAH dataset. JA ran the NOAH MP simulations. KR prepared the snow surface
584 properties dataset. EB processed the data and prepared the manuscript.

585 COMPETING INTERESTS

586 The authors declare that they have no conflicts of interest.

587 ACKNOWLEDGMENTS

588 We are grateful to the Aga Khan Agency for Habitat for supplying the first snow measurements in
589 Afghanistan's watersheds since the 1980s. This work was supported by NASA Awards
590 80NSSC18K0427, 80NSSC18K1489, NASA 2015 HiMAT, and NNX17AC15G.

591

592 REFERENCES

593 Adam, J. C., Clark, E. A., Lettenmaier, D. P., and Wood, E. F.: Correction of global precipitation
594 products for orographic effects, *Journal of Climate*, 19, 15-38, doi 10.1175/JCLI3604.1, 2006.

595 Armstrong, R. L., Rittger, K., Brodzik, M. J., and others: Runoff from glacier ice and seasonal snow in
596 High Asia: separating melt water sources in river flow, *Regional Environmental Change*, 1-13, doi
597 <https://doi.org/10.1007/s10113-018-1429-0>, 2018.

598 Bair, E. H., Davis, R. E., and Dozier, J.: Hourly mass and snow energy balance measurements from
599 Mammoth Mountain, CA USA, 2011–2017, *Earth Syst. Sci. Data*, 10, 549-563, doi 10.5194/essd-10-549-
600 2018, 2018a.

601 Bair, E. H., Simenhois, R., Birkeland, K., and Dozier, J.: A field study on failure of storm snow slab
602 avalanches, *Cold Regions Science and Technology*, 79-80, 20-28, doi 10.1016/j.coldregions.2012.02.007,
603 2012.

604 Bair, E. H., Abreu Calfa, A., Rittger, K., and Dozier, J.: Using machine learning for real-time estimates of
605 snow water equivalent in the watersheds of Afghanistan, *The Cryosphere*, 12, 1579-1594, doi 10.5194/tc-
606 12-1579-2018, 2018b.

607 Bair, E. H., Rittger, K., Skiles, S. M., and Dozier, J.: An Examination of Snow Albedo Estimates From
608 MODIS and Their Impact on Snow Water Equivalent Reconstruction, *Water Resources Research*, 55,
609 7826-7842, doi 10.1029/2019wr024810, 2019.

610 Bair, E. H., Rittger, K., Davis, R. E., Painter, T. H., and Dozier, J.: Validating reconstruction of snow
611 water equivalent in California's Sierra Nevada using measurements from the NASA Airborne Snow
612 Observatory, *Water Resources Research*, 52, 8437-8460, doi 10.1002/2016WR018704, 2016.

613 Bartelt, P., and Lehning, M.: A physical SNOWPACK model for the Swiss avalanche warning: Part I:
614 numerical model, *Cold Regions Science and Technology*, 35, 123-145, doi 10.1016/s0165-
615 232x(02)00074-5, 2002.

616 Bavay, M., and Egger, T.: MeteIO 2.4.2: a preprocessing library for meteorological data, *Geosci. Model*
617 *Dev.*, 7, 3135-3151, doi 10.5194/gmd-7-3135-2014, 2014.

618 Bellaire, S., Jamieson, J. B., and Fierz, C.: Forcing the snow-cover model SNOWPACK with forecasted
619 weather data, *The Cryosphere*, 5, 1115-1125, doi 10.5194/tc-5-1115-2011, 2011.

620 Bellaire, S., van Herwijnen, A., Bavay, M., and Schweizer, J.: Distributed modeling of snow cover
621 instability at regional scale, *Proceedings of the 2018 International Snow Science Workshop, Innsbruck,*
622 *Austria, 2018*, 871-875,

623 Bookhagen, B., and Burbank, D. W.: Toward a complete Himalayan hydrological budget: Spatiotemporal
624 distribution of snowmelt and rainfall and their impact on river discharge, *Journal of Geophysical*
625 *Research: Earth Surface*, 115, doi 10.1029/2009jf001426, 2010.

626 Broxton, P. D., Zeng, X., and Dawson, N.: Why Do Global Reanalyses and Land Data Assimilation
627 Products Underestimate Snow Water Equivalent?, *J. Hydrometeorol.*, 17, 2743-2761, doi 10.1175/jhm-d-
628 16-0056.1, 2016.

629 Burt, P., and Adelson, E.: The Laplacian pyramid as a compact image code, *IEEE Transactions on*
630 *Communications*, 31, 532-540, doi 10.1109/TCOM.1983.1095851, 1983.

631 Chabot, D., and Kaba, A.: Avalanche forecasting in the central Asian countries of Afghanistan, Pakistan
632 and Tajikistan, Proc. 2016 Intl. Snow Sci. Wksp., Breckenridge, CO, 2016,
633 <http://arc.lib.montana.edu/snow-science/item/2310>.

634 Chen, F., Barlage, M., Tewari, M., Rasmussen, R., Jin, J., Lettenmaier, D., Livneh, B., Lin, C., Miguez-
635 Macho, G., Niu, G.-Y., Wen, L., and Yang, Z.-L.: Modeling seasonal snowpack evolution in the complex
636 terrain and forested Colorado Headwaters region: A model intercomparison study, *Journal of Geophysical*
637 *Research: Atmospheres*, 119, 13,795-713,819, doi 10.1002/2014jd022167, 2014.

638 Cornwell, E., Molotch, N. P., and McPhee, J.: Spatio-temporal variability of snow water equivalent in the
639 extra-tropical Andes Cordillera from distributed energy balance modeling and remotely sensed snow
640 cover, *Hydrol. Earth Syst. Sci.*, 20, 411-430, doi 10.5194/hess-20-411-2016, 2016.

641 Cosgrove, B. A., Lohmann, D., Mitchell, K. E., Houser, P. R., Wood, E. F., Schaake, J. C., Robock, A.,
642 Marshall, C., Sheffield, J., Duan, Q., Luo, L., Higgins, R. W., Pinker, R. T., Tarpley, J. D., and Meng, J.:
643 Real-time and retrospective forcing in the North American Land Data Assimilation System (NLDAS)
644 project, *Journal of Geophysical Research: Atmospheres*, 108, 8842, doi 10.1029/2002JD003118, 2003.

645 Dahri, Z. H., Ludwig, F., Moors, E., Ahmad, B., Khan, A., and Kabat, P.: An appraisal of precipitation
646 distribution in the high-altitude catchments of the Indus basin, *Science of The Total Environment*, 548-
647 549, 289-306, doi <https://doi.org/10.1016/j.scitotenv.2016.01.001>, 2016.

648 Dahri, Z. H., Moors, E., Ludwig, F., Ahmad, S., Khan, A., Ali, I., and Kabat, P.: Adjustment of
649 measurement errors to reconcile precipitation distribution in the high-altitude Indus basin, *Int. J.*
650 *Climatol.*, 38, 3842-3860, doi 10.1002/joc.5539, 2018.

651 Dozier, J., and Frew, J.: Rapid calculation of terrain parameters for radiation modeling from digital
652 elevation data, *IEEE Transactions on Geoscience and Remote Sensing*, 28, 963-969, doi
653 10.1109/36.58986, 1990.

654 Dozier, J., Painter, T. H., Rittger, K., and Frew, J. E.: Time-space continuity of daily maps of fractional
655 snow cover and albedo from MODIS, *Advances in Water Resources*, 31, 1515-1526, doi
656 10.1016/j.advwatres.2008.08.011, 2008.

657 Ek, M. B., Mitchell, K. E., Lin, Y., Rogers, E., Grunmann, P., Koren, V., Gayno, G., and Tarpley, J. D.:
658 Implementation of Noah land surface model advances in the National Centers for Environmental
659 Prediction operational mesoscale Eta model, *Journal of Geophysical Research: Atmospheres*, 108, doi
660 10.1029/2002jd003296, 2003.

661 Fierz, C., Armstrong, R. L., Durand, Y., Etchevers, P., Greene, E., McClung, D. M., Nishimura, K.,
662 Satyawali, P. K., and Sokratov, S.: The International Classification for Seasonal Snow on the Ground,
663 IHP-VII Technical Documents in Hydrology N°83, 90, 2009.

664 Gelaro, R., McCarty, W., Suárez, M. J., Todling, R., Molod, A., Takacs, L., Randles, C. A., Darmenov,
665 A., Bosilovich, M. G., Reichle, R., Wargan, K., Coy, L., Cullather, R., Draper, C., Akella, S., Buchard,
666 V., Conaty, A., Silva, A. M. d., Gu, W., Kim, G.-K., Koster, R., Lucchesi, R., Merkova, D., Nielsen, J. E.,
667 Partyka, G., Pawson, S., Putman, W., Rienecker, M., Schubert, S. D., Sienkiewicz, M., and Zhao, B.: The
668 Modern-Era Retrospective Analysis for Research and Applications, Version 2 (MERRA-2), *Journal of*
669 *Climate*, 30, 5419-5454, doi 10.1175/jcli-d-16-0758.1, 2017.

670 Goodison, B., Louie, P. Y. T., and Yang, D.: WMO Solid precipitation measurement intercomparison,
671 World Meteorological Organization, 1998.

672 Harris, I., Jones, P. D., Osborn, T. J., and Lister, D. H.: Updated high-resolution grids of monthly climatic
673 observations – the CRU TS3.10 Dataset, *Int. J. Climatol.*, 34, 623-642, doi 10.1002/joc.3711, 2014.

674 Hirashima, H., Yamaguchi, S., Sato, A., and Lehning, M.: Numerical modeling of liquid water movement
675 through layered snow based on new measurements of the water retention curve, *Cold Regions Science
676 and Technology*, 64, 94-103, doi <https://doi.org/10.1016/j.coldregions.2010.09.003>, 2010.

677 Huffman, G. J., Bolvin, D. T., Nelkin, E. J., Wolff, D. B., Adler, R. F., Gu, G., Hong, Y., Bowman, K. P.,
678 and Stocker, E. F.: The TRMM Multisatellite Precipitation Analysis (TMPA): Quasi-Global, Multiyear,
679 Combined-Sensor Precipitation Estimates at Fine Scales, *J. Hydrometeorol.*, 8, 38-55, doi
680 10.1175/jhm560.1, 2007.

681 Immerzeel, W. W., Wanders, N., Lutz, A. F., Shea, J. M., and Bierkens, M. F. P.: Reconciling high-
682 altitude precipitation in the upper Indus basin with glacier mass balances and runoff, *Hydrol. Earth Syst.
683 Sci.*, 19, 4673-4687, doi 10.5194/hess-19-4673-2015, 2015.

684 Jamieson, J. B.: The compression test – after 25 years, *The Avalanche Review*, 18, 10-12, 1999.

685 Jepsen, S. M., Molotch, N. P., Williams, M. W., Rittger, K. E., and Sickman, J. O.: Interannual variability
686 of snowmelt in the Sierra Nevada and Rocky Mountains, United States: Examples from two alpine
687 watersheds, *Water Resources Research*, 48, W02529, doi 10.1029/2011WR011006, 2012.

688 Kochendorfer, J., Rasmussen, R., Wolff, M., Baker, B., Hall, M. E., Meyers, T., Landolt, S., Jachcik, A.,
689 Isaksen, K., Brækkan, R., and Leeper, R.: The quantification and correction of wind-induced precipitation
690 measurement errors, *Hydrol. Earth Syst. Sci.*, 21, 1973-1989, doi 10.5194/hess-21-1973-2017, 2017.

691 Lehning, M., Bartelt, P., Brown, B., and et. al: SNOWPACK model calculations for avalanche warning
692 based upon a new network of weather and snow stations, *Cold Reg. Sci. Technol.*, 30, 145-157, 1999.

693 Lehning, M., Bartelt, P., Brown, B., and Fierz, C.: A physical SNOWPACK model for the Swiss
694 avalanche warning: Part III: meteorological forcing, thin layer formation and evaluation, *Cold Regions
695 Science and Technology*, 35, 169-184, doi 10.1016/S0165-232X(02)00072-1, 2002a.

696 Lehning, M., Bartelt, P., Brown, B., Fierz, C., and Satyawali, P.: A physical SNOWPACK model for the
697 Swiss avalanche warning, Part II: Snow microstructure, *Cold Regions Science and Technology*, 35, 147-
698 167, doi: 110.1016/S0165-1232X(1002)00073-00073, 2002b.

699 Lehning, M., Völsch, I., Gustafsson, D., Nguyen, T. A., Stähli, M., and Zappa, M.: ALPINE3D: a
700 detailed model of mountain surface processes and its application to snow hydrology, *Hydrological
701 Processes*, 20, 2111-2128, doi 10.1002/hyp.6204, 2006.

702 Liston, G. E., and Elder, K.: A meteorological distribution system for high-resolution terrestrial modeling
703 (MicroMet), *J. Hydrometeorol.*, 7, 217–234, doi 10.1175/JHM486.1, 2006.

704 Lutz, A. F., Immerzeel, W. W., Shrestha, A. B., and Bierkens, M. F. P.: Consistent increase in High
705 Asia’s runoff due to increasing glacier melt and precipitation, *Nature Climate Change*, 4, 587, doi
706 10.1038/nclimate2237, 2014.

707 Margulis, S. A., Cortés, G., Giroto, M., and Durand, M.: A Landsat-Era Sierra Nevada Snow Reanalysis
708 (1985–2015), *J. Hydrometeorol.*, 17, 1203-1221, doi 10.1175/jhm-d-15-0177.1, 2016.

709 Marks, D., and Dozier, J.: Climate and energy exchange at the snow surface in the alpine region of the
710 Sierra Nevada, 2, *Snow cover energy balance*, *Water Resources Research*, 28, 3043-3054, doi
711 10.1029/92WR01483, 1992.

712 Martinec, J., and Rango, A.: Areal distribution of snow water equivalent evaluated by snow cover
713 monitoring, *Water Resources Research*, 17, 1480-1488, doi 10.1029/WR017i005p01480, 1981.

714 Milly, P. C. D., and Dunne, K. A.: Macroscale water fluxes I. Quantifying errors in the estimation of
715 basin mean precipitation, *Water Resources Research*, 38, 23-21-23-14, doi 10.1029/2001WR000759,
716 2002.

717 Mitterer, C., and Schweizer, J.: Analysis of the snow-atmosphere energy balance during wet-snow
718 instabilities and implications for avalanche prediction, *The Cryosphere*, 7, 205-216, doi 10.5194/tc-7-205-
719 2013, 2013.

720 Molotch, N. P.: Reconstructing snow water equivalent in the Rio Grande headwaters using remotely
721 sensed snow cover data and a spatially distributed snowmelt model, *Hydrological Processes*, 23, 1076-
722 1089, doi 10.1002/hyp.7206, 2009.

723 Monti, F., Schweizer, J., and Fierz, C.: Hardness estimation and weak layer detection in simulated snow
724 stratigraphy, *Cold Regions Science and Technology*, 103, 82-90, doi
725 <https://doi.org/10.1016/j.coldregions.2014.03.009>, 2014.

726 Nishimura, K., Baba, E., Hirashima, H., and Lehning, M.: Application of the snow cover model
727 SNOWPACK to snow avalanche warning in Niseko, Japan, *Cold Regions Science and Technology*, 43,
728 62-70, doi <https://doi.org/10.1016/j.coldregions.2005.05.007>, 2005.

729 Niu, G.-Y., and Yang, Z.-L.: Effects of vegetation canopy processes on snow surface energy and mass
730 balances, *Journal of Geophysical Research: Atmospheres*, 109, doi 10.1029/2004jd004884, 2004.

731 Niu, G.-Y., Yang, Z.-L., Mitchell, K. E., Chen, F., Ek, M. B., Barlage, M., Kumar, A., Manning, K.,
732 Niyogi, D., Rosero, E., Tewari, M., and Xia, Y.: The community Noah land surface model with
733 multiparameterization options (Noah-MP): 1. Model description and evaluation with local-scale
734 measurements, *Journal of Geophysical Research: Atmospheres*, 116, doi 10.1029/2010jd015139, 2011.

735 Painter, T. H., Bryant, A. C., and Skiles, S. M.: Radiative forcing by light absorbing impurities in snow
736 from MODIS surface reflectance data, *Geophysical Research Letters*, 39, L17502, doi
737 10.1029/2012GL052457, 2012.

738 Painter, T. H., Rittger, K., McKenzie, C., Slaughter, P., Davis, R. E., and Dozier, J.: Retrieval of subpixel
739 snow-covered area, grain size, and albedo from MODIS, *Remote Sensing of Environment*, 113, 868-879,
740 doi 10.1016/j.rse.2009.01.001, 2009.

741 Painter, T. H., Berisford, D. F., Boardman, J. W., Bormann, K. J., Deems, J. S., Gehrke, F., Hedrick, A.,
742 Joyce, M., Laidlaw, R., Marks, D., Mattmann, C., McGurk, B., Ramirez, P., Richardson, M., Skiles, S.
743 M., Seidel, F. C., and Winstral, A.: The Airborne Snow Observatory: Fusion of scanning lidar, imaging
744 spectrometer, and physically-based modeling for mapping snow water equivalent and snow albedo,
745 *Remote Sensing of Environment*, 184, 139-152, doi 10.1016/j.rse.2016.06.018, 2016.

746 Raup, B., Racoviteanu, A., Khalsa, S. J. S., Helm, C., Armstrong, R., and Arnaud, Y.: The GLIMS
747 geospatial glacier database: A new tool for studying glacier change, *Global and Planetary Change*, 56,
748 101-110, doi <https://doi.org/10.1016/j.gloplacha.2006.07.018>, 2007.

749 Rienecker, M. M., Suarez, M. J., Gelaro, R., Todling, R., Julio Bacmeister, Liu, E., Bosilovich, M. G.,
750 Schubert, S. D., Takacs, L., Kim, G.-K., Bloom, S., Chen, J., Collins, D., Conaty, A., Silva, A. d., Gu, W.,
751 Joiner, J., Koster, R. D., Lucchesi, R., Molod, A., Owens, T., Pawson, S., Pegion, P., Redder, C. R.,
752 Reichle, R., Robertson, F. R., Ruddick, A. G., Sienkiewicz, M., and Woollen, J.: MERRA: NASA's
753 Modern-Era Retrospective Analysis for Research and Applications, *Journal of Climate*, 24, 3624-3648,
754 doi 10.1175/jcli-d-11-00015.1, 2011.

755 Rittger, K., Bair, E. H., Kahl, A., and Dozier, J.: Spatial estimates of snow water equivalent from
756 reconstruction, *Advances in Water Resources*, 94, 345-363, doi 10.1016/j.advwatres.2016.05.015, 2016.

757 Rittger, K., Raleigh, M. S., Dozier, J., Hill, A. F., Lutz, J. A., and Painter, T. H.: Canopy Adjustment and
758 Improved Cloud Detection for Remotely Sensed Snow Cover Mapping, *Water Resources Research*, in
759 press.

760 Rodell, M., Houser, P. R., Jambor, U., Gottschalck, J., Mitchell, K., Meng, C. J., Arsenault, K., Cosgrove,
761 B., Radakovich, J., Bosilovich, M., Entin, J. K., Walker, J. P., Lohmann, D., and Toll, D.: The Global
762 Land Data Assimilation System, *Bulletin of the American Meteorological Society*, 85, 381-394, doi
763 10.1175/BAMS-85-3-381, 2004.

764 Rutan, D. A., Kato, S., Doelling, D. R., Rose, F. G., Nguyen, L. T., Caldwell, T. E., and Loeb, N. G.:
765 CERES synoptic product: Methodology and validation of surface radiant flux, *J. Atmos. Ocean. Technol.*,
766 32, 1121-1143, doi 10.1175/JTECH-D-14-00165.1, 2015.

767 Schweizer, J., and Jamieson, B.: Snow cover properties for skier triggering of avalanches, *Cold Regions
768 Science and Technology*, 33, 207-221, doi 10.1016/s0165-232x(01)00039-8, 2001.

769 Schweizer, J., and Jamieson, B.: A threshold sum approach to stability evaluation of manual snow
770 profiles, *Cold Regions Science and Technology*, 47, 50-59, doi 10.1016/j.coldregions.2006.08.011, 2007.

771 Shakoor, A., and Ejaz, N.: Flow Analysis at the Snow Covered High Altitude Catchment via Distributed
772 Energy Balance Modeling, *Scientific Reports*, 9, 4783, doi 10.1038/s41598-019-39446-1, 2019.

773 Skiles, S. M., and Painter, T.: Daily evolution in dust and black carbon content, snow grain size, and
774 snow albedo during snowmelt, *Rocky Mountains, Colorado, Journal of Glaciology*, 63, 118-132, doi
775 10.1017/jog.2016.125, 2016.

776 Smith, T., and Bookhagen, B.: Changes in seasonal snow water equivalent distribution in High Mountain
777 Asia (1987 to 2009), *Science Advances*, 4, e1701550, doi 10.1126/sciadv.1701550, 2018.

778 Sturm, M., Holmgren, J., and Liston, G. E.: A seasonal snow cover classification system for local to
779 global applications, *Journal of Climate*, 8, 1261-1283, doi 10.1175/1520-
780 0442(1995)008<1261:ASSCCS>2.0.CO;2, 1995.

781 Sturm, M., Taras, B., Liston, G. E., Derksen, C., Jonas, T., and Lea, J.: Estimating snow water equivalent
782 using snow depth data and climate classes, *J. Hydrometeorol.*, 11, 1380-1394, doi
783 10.1175/2010jhm1202.1, 2010.

784 Tan, B., Woodcock, C. E., Hu, J., Zhang, P., Ozdogan, M., Huang, D., Yang, W., Knyazikhin, Y., and
785 Myneni, R. B.: The impact of gridding artifacts on the local spatial properties of MODIS data:
786 Implications for validation, compositing, and band-to-band registration across resolutions, *Remote*
787 *Sensing of Environment*, 105, 98-114, doi 10.1016/j.rse.2006.06.008, 2006.

788 United Nations: Afghanistan: Nuristan avalanche, update to flash report (as of 8 February 2017), Office
789 for the Coordination of Humanitarian Affairs (OCHA), 2017.

790 USAID: Afghanistan Food Security Update, FEWS Net, Washington, DC, 4, 2008.

791 USGS: Global Land Survey: <http://glcfapp.glcf.umd.edu/data/gls/>, access: 1 September 2017, 2009.

792 van Herwijnen, A., and Jamieson, B.: Fracture character in compression tests, *Cold Regions Science and*
793 *Technology*, 47, 60-68, doi 10.1016/j.coldregions.2006.08.016, 2007.

794 Viste, E., and Sorteberg, A.: Snowfall in the Himalayas: an uncertain future from a little-known past, *The*
795 *Cryosphere*, 9, 1147-1167, doi 10.5194/tc-9-1147-2015, 2015.

796 Xia, Y., Mitchell, K., Ek, M., Sheffield, J., Cosgrove, B., Wood, E., Luo, L., Alonge, C., Wei, H., Meng,
797 J., Livneh, B., Lettenmaier, D., Koren, V., Duan, Q., Mo, K., Fan, Y., and Mocko, D.: Continental-scale
798 water and energy flux analysis and validation for the North American Land Data Assimilation System
799 project phase 2 (NLDAS-2): 1. Intercomparison and application of model products, *Journal of*
800 *Geophysical Research: Atmospheres*, 117, D03109, doi 10.1029/2011JD016048, 2012.

801 Xiaoxiong, X., Nianzeng, C., and Barnes, W.: Terra MODIS on-orbit spatial characterization and
802 performance, *IEEE Transactions on Geoscience and Remote Sensing*, 43, 355-365, doi
803 10.1109/TGRS.2004.840643, 2005.

804 Yang, Z.-L., and Niu, G.-Y.: The Versatile Integrator of Surface and Atmosphere processes: Part 1.
805 Model description, *Global and Planetary Change*, 38, 175-189, doi [https://doi.org/10.1016/S0921-](https://doi.org/10.1016/S0921-8181(03)00028-6)
806 [8181\(03\)00028-6](https://doi.org/10.1016/S0921-8181(03)00028-6), 2003.

807 Yatagai, A., Kamiguchi, K., Arakawa, O., Hamada, A., Yasutomi, N., and Kitoh, A.: APHRODITE:
808 Constructing a Long-Term Daily Gridded Precipitation Dataset for Asia Based on a Dense Network of
809 Rain Gauges, *Bulletin of the American Meteorological Society*, 93, 1401-1415, doi 10.1175/bams-d-11-
810 00122.1, 2012.
811